A new 2212-type stair like structure: $Bi_{14}Sr_{21}Fe_{12}O_{61}$, $m = 5$ member of the generic $[Bi_2Sr_3Fe_2O_9]_m[Bi_4Sr_6Fe_2O_{16}]$ family

M. Allix, O. Pérez, D. Pelloquin,* M. Hervieu, and B. Raveau

Laboratoire CRISMAT, UMR 6508-CNRS, ENSICAEN et Université de Caen, 6, Boulevard du Maréchal Juin, 14050 CAEN Cedex, France

Abstract

A new oxide, $Bi_{14}Sr_{21}Fe_{12}O_{61}$, with a layered structure derived from the 2212 modulated type structure $Bi_2Sr_3Fe_2O_9$, was isolated. It crystallizes in the $I2$ space group, with the following parameters: $a = 16.58(3)$ Å, $b = 5.496(1)$ Å, $c = 35.27(2)$ Å and $\beta = 90.62°$. The single crystal X-ray structure determination, coupled with electron microscopy, shows that this ferrite is the $m = 5$ member of the $[Bi_2Sr_3Fe_2O_9]_m[Bi_4Sr_6Fe_2O_{16}]$ collapsed family. This new collapsed structure can be described as slices of 2212 structure of five bismuth polyhedra thick along $\vec{a}$, shifted with respect to each other and interconnected by means of $[Bi_4Sr_6Fe_2O_{16}]$ slices. The latter are the place of numerous defects like iron or strontium for bismuth substitution; they can be correlated to intergrowth defects with other members of the family.
© 2004 Elsevier Inc. All rights reserved.

Keywords: Iron; Collapsed structure; Diffraction; $Bi_{14}Sr_{21}Fe_{12}O_{61}$; $Bi_2Sr_3Fe_2O_9$; Shearing phenomena

1. Introduction

Numerous layered oxides of the Bi–Sr–Fe–O system exhibit very close compositions. The pseudo ternary diagram shows indeed that small variations of the cation ratio and/or oxygen composition lead to different structures by intergrowth [1–3], ordered substitutions [4], $[AO]_\infty$ layer insertion [5–12] or shearing mechanisms inducing the formation of stair-like (also called collapsed) structures [13,14]. In contrast to bismuth based cuprates [15–17] only two bismuth ferrites with collapsed structures were characterized in spite of the great similarities of both systems. Only one $Bi_{12}Sr_{18}Fe_{10}O_{52}$ [14] was reported in the Bi–Sr–Fe–O system whereas the second containing barium, $Bi_{13}Ba_2Sr_{25}Fe_{13}O_{66}$ [18], is a 2201–0201 collapsed structure. $Bi_{12}Sr_{18}Fe_{10}O_{52}$ [14] was characterized by means of single crystal X-ray data and TEM techniques as the $m = 4$ member of the generic $[Bi_2Sr_3Fe_2O_9]_m[Bi_4Sr_6Fe_2O_{16}]$ 2212-type collapsed family.

This structural family can be described starting from the Bi-2212 structure [5,19] related to the ($n = 3/m = 2$) term of the large $Bi_{n-1}A_2A_{m-1}M_mO_{2m+n+1}$ series ($A =$ Sr, Ca… and $M =$ Cu, Fe, Co, Mn,…), i.e. the intergrowth between triple rock salt-type ($n = 3$) and double perovskite-type ($m = 2$) layers (Fig. 1a). A first shearing mechanism parallel to the stacking direction takes place periodically, every 4 octahedra along $\vec{a}$, in this ideal 2212-type framework and leads to a double (BiO) ribbon configuration in phase (Fig. 1b). A second mechanism associated to a gliding along $\vec{a}$-axis leads, at the level of the shearing zone, to a new structural stacking, involving the formation of perovskite-like blocks (Fig. 1c). This so-called collapsed structure is thus built up of $[Bi_2Sr_3Fe_2O_9]$ 2212-type slices, $m = 4$ octahedra wide interconnected through $[Bi_2Sr_3FeO_8]_\infty$ blocks, of $n = 2$ octahedra wide. The Bi/Fe ratio appears to be a very important parameter for stabilizing new members closed to the 2212 structure.

This paper deals with the structural study of a new ferrite, $Bi_{14}Sr_{21}Fe_{12}O_{61}$. From TEM observations, it can be described as a new member of the $[Bi_2Sr_3Fe_2O_9]_m[Bi_4Sr_6Fe_2O_{16}]$ 2212-type collapsed type family. The single crystal X-ray diffraction study allows

*Corresponding author. Fax: +33-2-31-96-16-00.
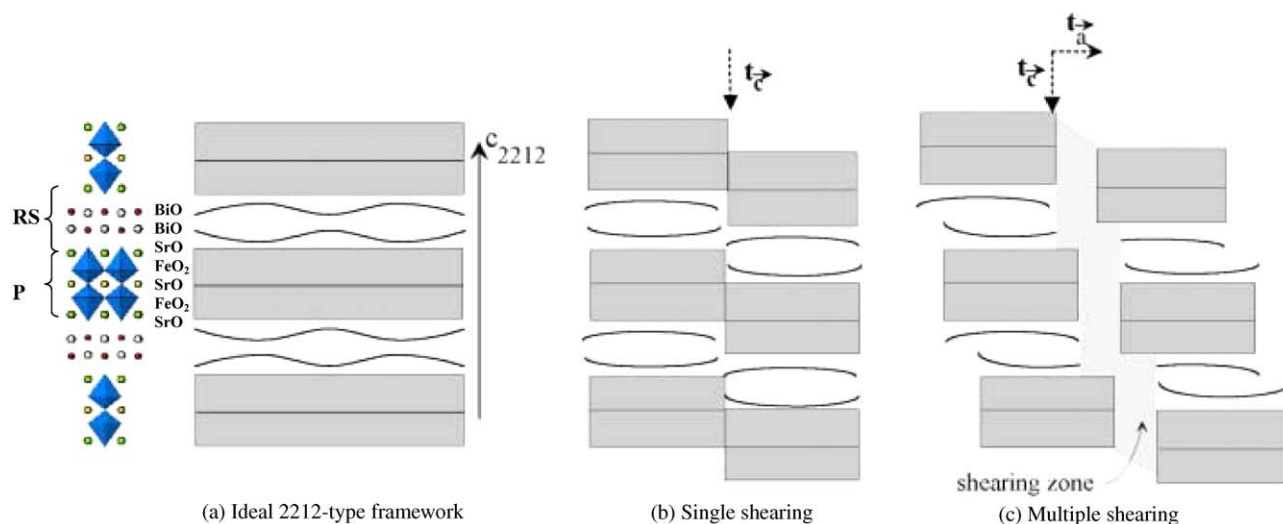 E-mail address: pelloquin@ismra.fr (D. Pelloquin).

Fig. 1. Ideal Bi-2212 stacking (a) and different structural mechanisms (b–c) leading to collapsed structures.

us to establish an accurate structure and the nature of the defects at the level of the sheared zones. The structure of this new collapsed layered oxide is discussed and compared with the previous results reported for $Bi_{12}Sr_{18}Fe_{10}O_{52}$ oxide [14].

2. Experimental section

2.1. Synthesis

Single crystals of the $Bi_{14}Sr_{21}Fe_{12}O_{61}$ phase were prepared from a mixture of Bi_2O_3, Fe, Fe_2O_3 and SrO, intimately ground in a dry box because of SrO oxide which must be freshly prepared by heating SrO_2 or $Sr(OH)_2, \cdot 8H_2O$ at 1100°C. The powder, with the nominal molar composition Bi:1.2 Sr:2.5 Fe:1 and O:5.7 was placed in an evacuated quartz ampoule and heated up to 1075°C during 6 h, held for 20 h and slowly cooled at 900°C during 24 h. It was finally cooled to room temperature at a rate of 150°C h^{-1}. By this way, single crystals in the form of brown needles were obtained.

2.2. Structural characterizations

The Electron Diffraction (E.D.) study was carried out using a JEOL 200CX microscope fitted with an eucentric goniometer ($\pm 60°$) while the High-Resolution Electron Microscopy (HREM) images were recorded with a TOPCON 002B microscope operating at 200 kV and having a point resolution of 1.8 Å. For the electron microscopy observations, crystals were crushed in butanol and the small flakes were deposited on a holey carbon film, supported by a copper grid. Energy Dispersive Spectroscopy (EDS) analyses were systematically carried out, both electron microscopes being

equipped with KEVEX analyzers. The HREM theoretical images were calculated using the Mac Tempas multi-slice program [20], varying the focus values and crystal thickness and using the atomic positions obtained from X-ray single crystal refinements.

The X-ray diffraction data were collected at room temperature with a four circle X-ray diffractometer equipped with a CCD detector (Kappa CCD Bruker-Nonius) using MoKα radiation. The structure was solved with the SIR2002 [21] program and refined using the JANA2000 [22] software.

A preliminary X-ray investigation was performed at room temperature to explore the diffraction pattern of the present compound. Large Ω and Φ scans were used to control the crystalline quality of different samples and to determine cell parameters. A single crystal of suitable size ($0.260 \times 0.025 \times 0.015$ mm^3) was then selected; note that the whole crystal exhibits a needle shape. Frames were collected, for $0 < \theta < 30°$, with a classical "$\Phi - \Omega$" scans strategy, a small scan angle (0.3°/frame) and a short sample-detector distance (Dx = 34 mm). The precession pictures calculated from these series of experimental frames are sufficiently accurate to obtain an overall view of the reciprocal space.

On the basis of the precession pictures, a suitable data collection strategy was defined. Owing to the cell parameters and the spot size, a scanning angle of 0.4° and a Dx value of 60 mm were chosen; $\Phi - \Omega$ scans were used. In order to gather greater number of reflections but avoiding any detector saturation by reflections of strong intensity, two different exposure times (150 s/° and 15 s/°) were used to collect data at room temperature. The diffracted intensities were collected up to $\theta = 42°$. A redundancy of 2.2 for 90% of the reflections was reached. The EvalCCD software [23] was used to extract reflections from the collected frames; reflections were

Table 1
Crystal data

Crystal color	Brown
Density	$6.75 \, \text{g cm}^3$
Laue class	$2/m$
Cell parameters (Å)	
a	16.553(6)
b	5.495(2)
c	35.305(5)
β (deg)	90.57(8)
Space group	$I2$
Unique reflections with $I \geqslant 3\sigma(I)$	11207
Reflection limits	
$-31 \leqslant h \leqslant 31$	
$0 \leqslant k \leqslant 10$	
$0 \leqslant l \leqslant 66$	
Absorption coefficient	$59.28 \, \text{mm}^{-1}$
Internal R factor (%)	4.8
Weighting scheme	unitary
Refinement parameters	346
Reliability factor (%)	5.2
Refined composition	$Bi_{14.87(5)}Sr_{20.25(5)}Fe_{11.88(6)}O_{61}$

merged and rescaled as a function of the exposure time. Data were corrected for Lorentz, polarization and absorption using Jana2000 program [21] within the analytical option based on the crystal morphology. The crystal data are gathered in the Table 1.

3. Results

3.1. Chemical composition and stacking mode

Several crystals were selected in the batch in order to determine the actual cationic composition. EDS analysis lead to the average cationic composition $Bi_{2.06}Sr_{3.19}Fe_{1.75}$ which is iron deficient with regard to the ideal 2212 structure, namely $Bi_2Sr_3Fe_2$.

The single crystal X-ray diffraction patterns and E.D. patterns are similar. They evidence the co-existence of two systems of reflections: one system of intense reflections consistent with a 2212-type subcell (Fig. 2) and a system of weaker satellites. They allow us to characterize a monoclinic cell and, among the different possible cells, a β value close to 90° was chosen for reducing the correlation between x and z atomic parameters during the refinement. As a consequence, a monoclinic cell with $\beta \approx 90°$ and the following parameters: $a \approx 7 \times a_p\sqrt{2} \approx 35$, $b \approx a_p\sqrt{2}$ and $c \approx 16.5$ Å was chosen. The complex [010] (Fig. 2a) oriented E.D. patterns are characteristic of modulated bismuth based layered oxides [5–18]. The reflection condition, hkl: $h + k + l = 2n$ is consistent with the space groups $I2/m$ and $I2$.

The parameters and symmetry of the title compound can be compared to that determined for the collapsed $Bi_{12}Sr_{18}Fe_{10}O_{52}$ [13,14] oxide and ascribed to a complex

shearing mechanism along $\vec{a}$ leading to 2212-type slices 4 octahedra wide interconnected by $[Bi_2Sr_3FeO_8]_\infty$ slices (2 octahedra wide). In order to understand the stacking mode of this layered iron oxide and to characterize the collapsed mechanism, a HREM study was performed. The appropriate information's are obtained in the [010] oriented images. This is illustrated in Fig. 3 where high electron density zones appear as bright dots (close to -550 Å) in the thin part of the crystal edge. In such an image, the undulation of the atomic layers is clearly visible, as well as the breaking of the dots intensity along [100], due to the shearing mechanism. The layer stacking mode can be determined by viewing locally the relative arrangement of the bright and gray dots: quadruple rows of bright dots in staggered positions alternate with one single row of bright dots sandwiched by two single rows of darker spots. The brighter dots are correlated to the Bi and Sr layers and the gray ones to the iron ones. Such a description involves the local sequence $[SrO]_\infty$ $[BiO]_\infty [BiO]_\infty [SrO]_\infty [FeO_2]_\infty [SrO]_\infty [FeO_2]_\infty$ along the direction perpendicular to the different atomic layers,
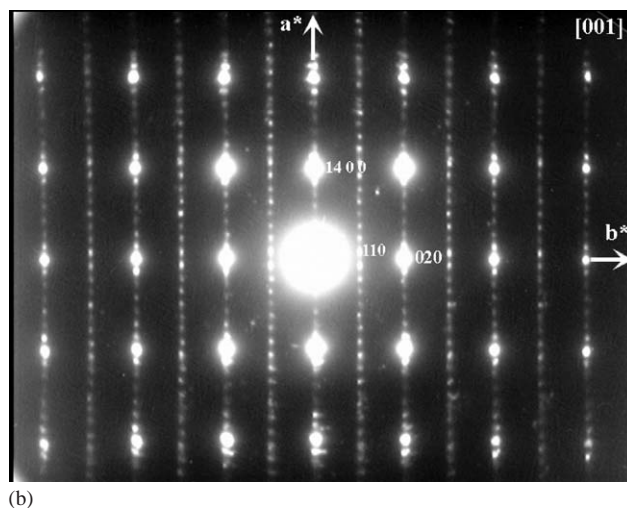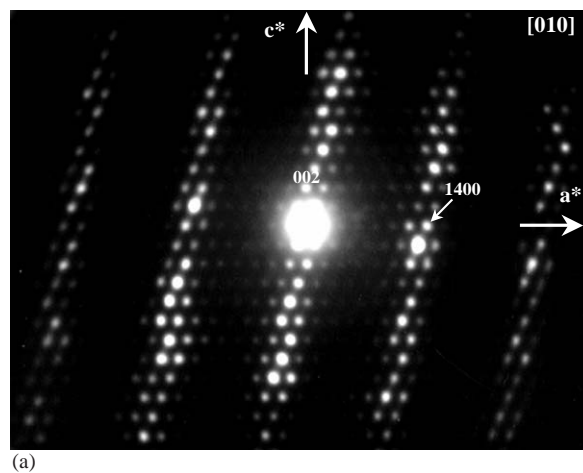

(a)

(b)

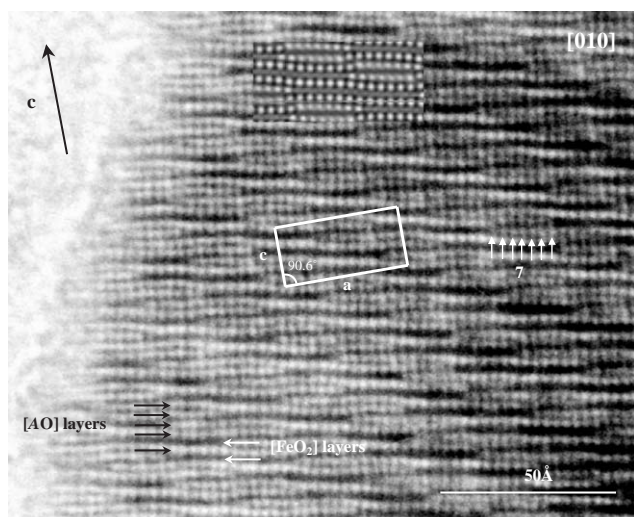Fig. 2. Experimental (a) [010] and (b) [001] E.D. patterns of $Bi_{14}Sr_{21}Fe_{12}O_{61}$ oxide.

Fig. 3. Experimental [010] HREM image of $Bi_{14}Sr_{21}Fe_{12}O_{61}$ oxide recorded with a defocus value close to $-550\,\text{Å}$. The simulated image from atomic positions given in Table 2 with a crystal thickness close to $30\,\text{Å}$ is embedded.

i.e. in agreement with the 2212-type stacking mode. The shearing mechanism breaks the infinite character of the layers along a_{2212} and b_{2212}, giving to them a stair-like configuration similar to that previously reported for $Bi_{12}Sr_{18}Fe_{10}O_{52}$ [13–14]. However, this image shows also that this shearing mechanism induces a different periodicity of 7 bright dots, spaced at about $a_p\sqrt{2}/2 \approx 2.7\,\text{Å}$, along b_{2212} (white arrows Fig. 3). This periodicity can be compared to the $6a_p\sqrt{2}/2$ bright dots observed in $Bi_{12}Sr_{18}Fe_{10}O_{52}$ [13–14] oxide. In the latter these contrasts are correlated to slices which have 4 and 2 octahedra thick in agreement with the $m = 4$ member of the $[Bi_2Sr_3Fe_2O_9]_m[Bi_4Sr_6Fe_2O_{16}]$ collapsed family. By analogy, this new sheared structure can be described as the $m = 5$ member of this family. Note that the general formulation of this family induces a common Bi/Sr ratio whatever the m value, the main difference staying in the iron and oxygen contents. The experimental average cationic composition, $Bi_{13.8}Sr_{21.4}Fe_{11.8}$, is indeed close to the theoretical one $Bi_{14}Sr_{21}Fe_{12}$ ($m = 5$) and within the limit of accuracy of the EDS technique. The crystal growth of $m = 5$ member provides the opportunity to understand the difference and similarities between the mother 2212-type structure and the different collapsed members. An accurate structural determination has therefore been carried out by X-ray diffraction and in a second step the selected crystal was crushed and characterized by HREM.

3.2. Structure refinements

A structural model considering the $I2/m$ space group was built with SIR2002 using direct methods. 24 cations were located leading to a reliability factor of 38%. The main problem of this solution is, in fact, linked to the coloring of the different atomic sites. A rapid comparison with the structure of the $m = 4$ member [14] helps us to assign the right atomic species to all the sites; the reliability factor decreases down to 28%. The model is then introduced in the refinement program Jana2000. Using Fourier difference series, 31 oxygen positions are found. Anisotropic displacement parameters (ADP) were considered for all the cations; note that all these sites were located in the mirror m perpendicular to the b-axis. The refinement of the ADP leads to very large values for U_{22} (up to $0.17\,\text{Å}^2$) for all the Bi and some Sr atoms. These anomalies were already observed for the "collapsed" $m = 4$ study; they were mainly due to bismuth displacements from their ideal position in the m mirror perpendicular to b. These displacements induce a lowering of symmetry from $B2/m$ to $P2_1/n$. In the present case, no extra reflection allows us to reject the I centred lattice and then the m mirror. Only the noncentro symmetric hypothesis, in the $I2$ space group, allows this mirror to be removed and then makes possible atomic displacements without restrain on the y coordinates. Choosing an unitary weighting scheme to increase the relative weight of weak reflections, a first model with isotropic thermal motions fixed to reasonable values was introduced in the $I2$ space group. Displacement of bismuth along b from its ideal position ($y = 0$) was initiated by trial and error method. ADP were considered for all the cations and isotropic displacement parameters for oxygen atoms. They were refined to correct values; no anomaly is observed anymore. Moreover, while the reliability factor obtained in the centrosymmetric hypothesis was equal to 17%, it decreases now to below 10% using the $I2$ S.G. A projection along b of the structure is drawn in Fig. 4; the name of all the atoms are given. At this step of the refinement substitutions of Bi for Sr and the reciprocal were introduced; they are significant for some atoms. Finally, Fourier difference series were calculated; they reveal the existence of relatively strong electronic residues close to the Bi(1) and Sr(11) atoms. Note that, for these atoms, the refined occupancy was found inferior to 1. Two new atomic sites, X and Y, were then introduced in place of the two residues. Owing to the position of these two sites in the structure (close to a $[FeO_2]$ and to a $[BiO]$ ribbon respectively), X was considered as an iron atom and Y as a bismuth atoms; the X–O and Y–O distances corresponding to Fe–O and Bi–O distances respectively, this assumption seems to be reasonable. To illustrate our remarks on these sites, the density corresponding to the Y and Sr(11) sites are drawn in Fig. 4. Note that the X and Y sites occupancies were refined and have lead to values close to 1/6.

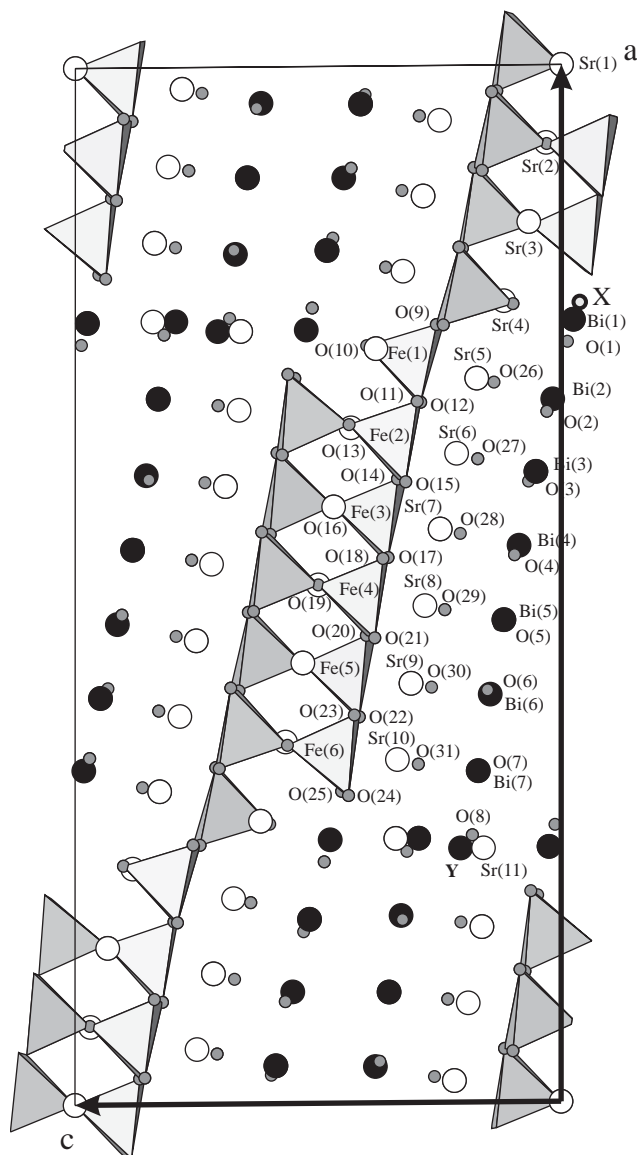The final refinement leads to an agreement factor equal to 5.2%; Results are summarized in Tables 2 and 3 (Fig. 5).

Fig. 4. Projection along b of the collapsed structure $Bi_{14}Sr_{21}Fe_{12}O_{61}$. Names of all the atomic sites considered in the refinement are summarized.

4. Discussion

The single crystal X-ray diffraction study allowed a satisfactory model to be reached. The final refined cation positions (Table 2) were used for HREM images calculations. The example of simulated [010] image (focus = $-550\,\text{Å}$ and thickness = $50\,\text{Å}$) embedded in the Fig. 3 fits well the experimental one. Thus this structural model extends the formation mechanism of the collapsed structure firstly proposed for the $Bi_{12}Sr_{18}Fe_{10}O_{52}$ oxide [13,14]. The two structural models of $Bi_{12}Sr_{18}Fe_{10}O_{52}$, $m = 4$, and $Bi_{14}Sr_{21}Fe_{12}O_{61}$, $m = 5$ members of the collapsed $[Bi_2Sr_3Fe_2O_9]_m[Bi_4Sr_6Fe_2O_{16}]$ family are compared in Fig. 6a and b.

The structure of these collapsed phases was described in the introduction part as the intergrowth between "2212" slices of variable thickness and slabs related to $Bi_2Sr_3FeO_8$. The 2212-type slices can be identified as 5 Fe polyhedra wide for $Bi_{14}Sr_{21}Fe_{12}O_{61}$ and 4 polyhedra wide for $Bi_{12}Sr_{18}Fe_{10}O_{52}$. Two successive "2212" slices are shifted with respect to each other by roughly $1/8(c_{2212})$ and are connected via intermediate zones of composition $Bi_4Sr_6Fe_2O_{12}$. In fact, the building of these structural frameworks does not result from a simple shearing mechanism. To obtain an accurate understanding of the mechanism leading to these collapsed phases, a comparison with the structural features of the parent $Bi_2Sr_3Fe_2O_9$ modulated "2212" compound is primordial (Fig. 1a). Owing to the modulation, the atoms form undulated layers along c_{2212}; these layers are composed of only one cation species (Bi, Sr or Fe). Owing to the symmetry of the "2212" phases, the modulation of two adjacent slabs is out of phase. This feature gives rise, to two adjacent [BiO] layers, to shrinking and bulging inducing Bi-diluted and Bi-condensed regions within each [BiO] layers. The Bi-diluted regions correspond to zones where the Bi–Bi distances within a same layer are maximal. In Fig. 7a, the position electronic lone pairs (Lp) of Bi^{3+}, calculated by electrostatic interaction, are drawn for a double [BiO] layer. The role played by the lone pairs, notably in the bulging zones, to fix both the peculiar structure of the double [BiO] layers and the modulation in this compound is then clearly outlined. The Bi-diluted (shrinking) zones, located on each side of a bulging zone, allow the strains to be released. For the "stair"-like phases, an iron sub-stoichiometry can be evidenced; the ideal $m = 4$ and 5 members of the family are in agreement with the chemical formula $Bi_2Sr_3Fe_{1.67}O_{8.67}$ and $Bi_2Sr_3Fe_{1.71}O_{8.71}$ respectively instead of $Bi_2Sr_3Fe_2O_9$ for the modulated parent compound. This sub-stoichiometry leads along b_{2212} to mixed cationic (Bi, Sr, Fe) layers. The "2212" blocks, identified below, correspond only to the bulging zone of the "2212" modulated slabs; consequently the Bi-diluted zones are absent in the "stair"-like phases. In the latter, the Lp configuration for a double [BiO] ribbon is shown in the Fig. 7b. In this type of structures where Bi-diluted zones, i.e. relaxation regions, do not exist, the shift evidenced between two adjacent blocks make it possible a minimization of the Lp interactions.

The analysis of distances evidences several structural features. First iron species exhibit a 5 + 1 coordination instead of true octahedral coordination with four equatorial bonds ranging from 1.89 to 1.96 Å, a typical apical bond close to 2 Å and a greater one (2.5 Å). So the iron polyhedra are mainly pyramidal. The bismuth species environment is a function of their location in the structure. The atoms located in the middle of the 2212-type slices, namely Bi(5) and Bi(6) in Table 3, are

Table 2
Atomic positions

Atoms	x	y	z	$U_{\text{iso}}(\text{Å}^2)$	Occupation
Bi1	−0.02481(5)	0	0.75409(3)	0.0092(2)	0.84
X	−0.0156(11)	0.007(5)	0.7649(7)	0.0092(2)	0.16
Bi2	0.01769(4)	0.4851(3)	0.67753(2)	0.01148(17)	1
Bi3	0.05215(5)	0.0175(4)	0.60769(3)	0.0130(2)	1
Bi4	0.08675(4)	0.4722(4)	0.53658(3)	0.01135(19)	1
Bi5	0.11800(4)	0.0278(4)	0.46495(3)	0.0112(2)	1
Bi6/Sr	0.14609(5)	0.4670(4)	0.39322(3)	0.0140(2)	0.95/0.05
Bi7/Sr	0.17068(5)	0.0114(4)	0.31951(3)	0.0100(2)	0.67/0.33
Sr1	0	−0.0128(10)	0	0.0097(5)	1
Sr2	0.03164(11)	0.4821(7)	0.92485(5)	0.0102(4)	1
Sr3	0.06715(13)	−0.0084(7)	0.84875(6)	0.0159(5)	1
Sr4	0.11856(14)	0.4915(7)	0.77259(6)	0.0173(5)	1
Sr5	0.17394(11)	−0.0072(7)	0.69814(5)	0.0115(5)	1
Sr6	0.21538(11)	0.5006(7)	0.62577(6)	0.0158(5)	1
Sr7	0.24913(10)	−0.0058(7)	0.55292(5)	0.0130(5)	1
Sr8	0.28049(11)	0.5042(7)	0.47915(5)	0.0154(5)	1
Sr9	0.30899(12)	−0.0085(8)	0.40433(5)	0.0139(5)	1
Sr10	0.33700(14)	0.4904(7)	0.33092(5)	0.0217(5)	1
Sr11	0.34019(17)	−0.0156(6)	0.25492(6)	0.0120(5)	0.83
Bi8	0.2931(5)	−0.0181(18)	0.25486(15)	0.030(2)	0.17
Fe1	0.27962(18)	0.4950(9)	0.71365(8)	0.0156(6)	1
Fe2	0.32485(14)	−0.0054(10)	0.63920(8)	0.0086(3)	1
Fe3	0.35829(15)	0.4924(10)	0.56442(8)	0.0086(3)	1
Fe4	0.38827(15)	−0.0025(11)	0.48888(8)	0.0091(5)	1
Fe5	0.41769(15)	0.4933(10)	0.41317(8)	0.0086(3)	1
Fe6	0.44508(14)	−0.0040(7)	0.33283(10)	0.0308(8)	1
O1	0.0125(10)	0.419(3)	0.2671(5)	0.023(3)	1
O2	0.9702(10)	0.103(3)	0.3344(5)	0.016(3)	1
O3	0.9327(9)	0.390(3)	0.4015(5)	0.013(3)	1
O4	0.9040(14)	0.095(5)	0.4725(7)	0.030(5)	1
O5	0.1270(11)	0.406(4)	0.4600(6)	0.022(3)	1
O6	0.1516(10)	0.089(3)	0.3974(5)	0.017(3)	1
O7	0.1738(13)	0.391(5)	0.3235(7)	0.032(4)	1
O8	0.1826(9)	0.020(4)	0.2577(5)	0.023(3)	1
O9	0.7571(8)	0.253(3)	0.2501(5)	0.006(2)	1
O10	0.5996(8)	0.482(5)	0.2697(5)	0.015(2)	1
O11	0.7894(12)	0.253(4)	0.1753(6)	0.015(4)	1
O12	0.7035(9)	0.245(2)	0.3237(4)	0.007(2)	1
O13	0.0632(7)	0.497(5)	0.8456(4)	0.014(2)	1
O14	0.8368(8)	0.246(2)	0.1015(4)	0.006(2)	1
O15	0.6799(8)	0.243(2)	0.4012(4)	0.005(2)	1
O16	0.5304(6)	0.474(3)	0.4239(3)	0.010(2)	1
O17	0.8564(10)	0.249(3)	0.0259(5)	0.010(3)	1
O18	0.6332(10)	0.252(3)	0.4751(5)	0.010(3)	1
O19	0	0.492(7)	0	0.020(4)	1
O20	0.3837(8)	0.248(2)	0.4485(4)	0.0047(19)	1
O21	0.0992(7)	0.250(2)	0.0491(3)	0.0025(17)	1
O22	0.0845(9)	0.246(3)	0.1277(5)	0.009(2)	1
O23	0.4256(13)	0.251(4)	0.3744(7)	0.025(4)	1
O24	0.4377(9)	0.237(3)	0.2966(5)	0.014(2)	1
O25	0.0484(13)	0.216(4)	0.1992(7)	0.025(4)	1
O26	0.6386(9)	0.008(5)	0.1941(5)	0.017(3)	1
O27	0.6720(8)	0.462(4)	0.1203(5)	0.015(3)	1
O28	0.7077(8)	0.030(3)	0.0485(4)	0.011(2)	1
O29	0.2605(8)	0.489(5)	0.0249(4)	0.016(2)	1
O30	0.2332(9)	0.025(4)	0.0995(5)	0.017(3)	1
O31	0.2062(11)	0.477(6)	0.1737(6)	0.029(4)	1

surrounded by four oxygens ranging from 2.05 to 2.5 Å, while those in periphery, namely Bi(2), Bi(3), Bi(4) and Bi(7), have five oxygen neighbors ranging from 2.05 to 2.25 Å. Considering their electronic lone pair $6s^2$(Lp), they exhibit pyramidal BiO_4L and tetrahedral BiO_3L coordinations, respectively. Such bismuth environments

Table 3
Main atomic distances

Bi1–O10i	2.128(14)	Bi2–O26ii	2.083(14)	Bi4–O28ii	2.066(13)	Bi6–O30xi	2.037(15)
Bi1–O8iv	2.642(15)	Bi2–O3iii	2.962(17)	Bi4–O3iii	2.256(17)	Bi6–O5	2.40(2)
Bi1–O24i	2.177(16)	Bi2–O2iii	2.147(18)	Bi4–O4iii	2.10(3)	Bi6–O6	2.085(18)
Bi1–O1iv	2.429(19)	Bi2–O1iv	2.055(19)	Bi4–O5	2.81(2)	Bi6–O7	2.54(3)
Bi1–O25iv	2.07(2)						
		Bi3–O27i	2.051(14)	Bi5–O4iii	2.27(3)	Bi7–O6	2.802(18)
Bi1–X	0.41(2)	Bi3–O3iii	2.087(18)	Bi5–O5	2.09(2)	Bi7–O8	2.193(17)
X–O10i	1.92(2)	Bi3–O2iii	2.134(18)	Bi5–O6	2.476(18)	Bi7–O31viii	2.058(18)
X–O8iv	2.87(2)	Bi3–O4iii	2.96(3)	Bi5–O29viii	2.050(13)	Bi7–O7	2.09(3)
X–O24i	2.01(3)						
X–O1iv	2.53(3)						
X–O25iv	1.80(3)						
Sr1–O17ix	2.931(16)	Sr2–O13	2.851(15)	Sr3–O13x	2.72(3)	Sr4–O13	2.743(15)
Sr1–O17xiii	2.931(16)	Sr2–O14iii	2.707(14)	Sr3–O13	2.78(3)	Sr4–O11iii	2.71(2)
Sr1–O18xiv	2.709(16)	Sr2–O17iii	2.834(17)	Sr3–O14iii	2.740(14)	Sr4–O26ii	2.793(18)
Sr1–O18viii	2.709(16)	Sr2–O15ii	2.966(13)	Sr3–O11iii	2.91(2)	Sr4–O9ii	2.824(15)
Sr1–O19x	2.72(4)	Sr2–O18ii	2.846(16)	Sr3–O15i	2.952(14)	Sr4–O9iii	2.573(15)
Sr1–O19	2.77(4)	Sr2–O19xvi	2.709(2)	Sr3–O12i	2.782(15)	Sr4–O12ii	2.670(15)
Sr1–O20xiv	2.944(13)	Sr2–O20ii	2.976(13)	Sr3–O16i	2.727(12)	Sr4–O10i	2.82(3)
Sr1–O20viii	2.944(13)	Sr2–O21iv	2.680(12)	Sr3–O22iv	2.997(15)	Sr4–O10ii	2.71(3)
Sr1–O21	2.782(12)	Sr2–O16i	2.789(19)	Sr3–O10i	2.847(16)	Sr4–O24ii	3.396(16)
Sr1–O21xv	2.782(12)	Sr2–O16ii	2.701(19)	Sr3–O23i	2.84(2)	Sr4–O1iv	2.602(18)
Sr1–O16xiv	2.740(12)	Sr2–O22iv	2.957(16)	Sr3–O24i	3.138(16)	Sr4–O25iv	3.31(2)
Sr1–O16viii	2.740(12)	Sr2–O23ii	2.89(2)	Sr3–O25iv	2.82(2)		
Sr5–O11i	2.46(2)	Sr6–O14ii	2.571(14)	Sr7–O14i	2.619(14)	Sr8–O17ii	2.464(17)
Sr5–O26i	2.73(3)	Sr6–O28ii	2.733(15)	Sr7–O17i	2.429(16)	Sr8–O28ii	2.742(15)
Sr5–O26ii	2.89(3)	Sr6–O11ii	2.54(2)	Sr7–O28ii	2.643(18)	Sr8–O29viii	2.91(3)
Sr5–O9i	2.637(16)	Sr6–O26ii	2.737(17)	Sr7–O28ii	3.025(18)	Sr8–O29xi	2.75(2)
Sr5–O9iii	2.576(16)	Sr6–O15iii	2.439(14)	Sr7–O29viii	2.751(16)	Sr8–O18iii	2.556(16)
Sr5–O12iii	2.580(15)	Sr6–O12iii	2.627(15)	Sr7–O15iii	2.414(14)	Sr8–O20	2.469(13)
Sr5–O27i	2.751(17)	Sr6–O27i	3.05(2)	Sr7–O18iii	2.608(16)	Sr8–O21xi	2.613(12)
Sr5–O10i	2.819(16)	Sr6–O27ii	2.64(2)	Sr7–O27i	2.716(16)	Sr8–O30xi	2.786(17)
Sr5–O2iii	2.707(17)	Sr6–O3iii	2.694(16)	Sr7–O4iii	2.74(2)	Sr8–O5	2.678(18)
Sr9–O29viii	2.758(15)	Sr10–O30xi	2.733(17)	Sr11–O8	2.618(16)		
Sr9–O20	2.431(14)	Sr10–O22xi	2.401(16)	Sr11–O8viii	2.62(2)		
Sr9–O21viii	2.591(12)	Sr10–O23	2.49(2)	Sr11–O8xi	3.00(2)		
Sr9–O30viii	2.66(2)	Sr10–O8xi	3.145(17)	Sr11–O31viii	2.64(2)		
Sr9–O30xi	3.02(2)	Sr10–O31viii	2.91(3)	Sr11–O7viii	2.82(3)		
Sr9–O22viii	2.497(15)	Sr10–O31xi	2.77(3)	Sr11–O24	2.579(16)		
Sr9–O23	2.63(2)	Sr10–O7	2.77(2)	Sr11–O1viii	2.589(18)		
Sr9–O6	2.667(16)	Sr10–O24	2.493(16)	Sr11–O25viii	2.85(2)		
Sr9–O31viii	2.76(2)	Sr10–O25xi	2.51(2)	Sr11–Bi8	0.779(8)		
Fe1–O11ii	1.97(2)	Fe2–O13xvii	1.923(13)	Fe3–O14ii	1.943(14)	Fe4–O17i	1.965(17)
Fe1–O26ii	2.428(15)	Fe2–O14i	1.920(14)	Fe3–O17ii	1.957(17)	Fe4–O29viii	2.505(13)
Fe1–O9ii	1.950(16)	Fe2–O11i	1.94(2)	Fe3–O28ii	2.558(13)	Fe4–O18iii	1.923(17)
Fe1–O9iii	1.948(16)	Fe2–O15iii	1.973(14)	Fe3–O15iii	1.940(14)	Fe4–O19xviii	1.887(3)
Fe1–O12iii	1.924(15)	Fe2–O12iii	1.960(15)	Fe3–O18iii	1.927(17)	Fe4–O20	1.981(14)
Fe1–O10iii	2.080(14)	Fe2–O27i	2.616(14)	Fe3–O16iii	1.887(11)	Fe4–O21viii	1.921(13)
Fe5–O20	1.923(14)	Fe5–O16	1.902(11)	Fe6–O13xix	2.002(13)	Fe6–O31viii	2.513(18)
Fe5–O21xi	1.962(13)	Fe5–O22xi	2.003(16)	Fe6–O22viii	2.018(16)	Fe6–O24	1.843(16)
Fe5–O30xi	2.539(15)	Fe5–O23	1.91(2)	Fe6–O23	2.06(2)	Fe6–O25viii	1.91(2)

Symmetry code: i = −1/2 + x, −1/2 + y, 1/2 + z; ii = −1/2 + x, 1/2 + y, 1/2 + z; iii = 3/2 − x, 1/2 + y, 3/2 − z; iv = 1/2 − x, 1/2 + y, 3/2 − z; v = 1/2 − x, −1/2 + y, 3/2 − z; vi = 3/2 − x, 3/2 + y, 3/2 − z; vii = 3/2 − x, −1/2 + y, 3/2 − z; viii = −x, −1 + y, −z; ix = −1 + x, y, z; x = x, −1 + y, z; xi = −x, y, −z; xii = x, 1 + y, z; xiii = 3/2 − x, 1/2 + y, 1/2 − z; xiv = −1/2 + x, −1/2 + y, −1/2 + z; xv = 1/2 − x, 1/2 + y, 1/2 − z; xvi = x, y, 1 + z; xvii = −x, −1 + y, 1 − z; xviii = 1/2 + x, −1/2 + y, 1/2 + z; xix = 1/2 + x, −1/2 + y, −1/2 + z.
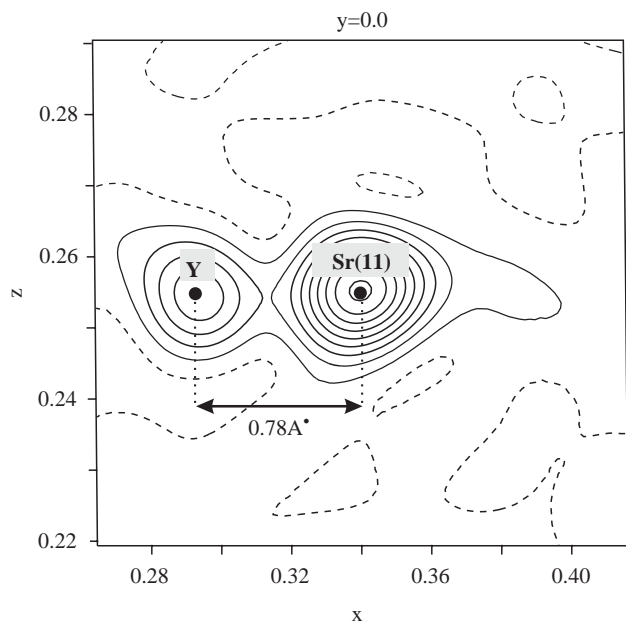
Fig. 5. Observed Fourier map showing up the Sr(11) and Y sites. Solid and dashed lines represent positive and negative density respectively. Contours are drawn at intervals of $3e^-/Å^3$.
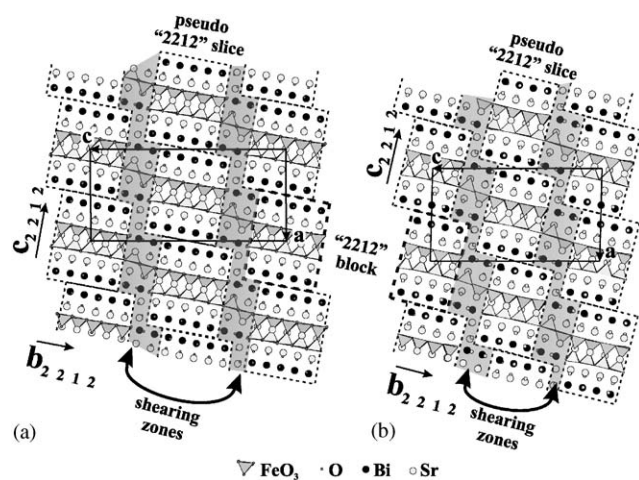

Fig. 6. Projection along b of the $m = 5$ (a) and $m = 4$ (b) collapsed structures.

Fig. 7. Lone pair (Lp) position for [BiO] layers in $Bi_2Sr_3Fe_2O_9$ modulated phase (a) and for [BiO] ribbon in $Bi_{12}Sr_{18}Fe_{10}O_{52}$ "terrace"-like phase.
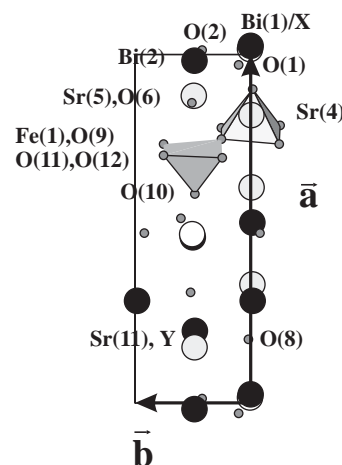
Fig. 8. Projection along c of the intermediate $Bi_4Sr_6Fe_2O_{12}$ zone.

are consistent with those observed in the 2212-type modulated structures. The description of the Bi(1) sitting in the shearing zone is more complex since iron was detected in the same site. In fact this site forms a junction with the adjacent [FeO$_2$] layer. Consequently Bi(1) exhibits three short in-plane bonds, ranging from 2.07 to 2.18 Å, with O(10), O(24) and O(25) but also two long apical bonds, ranging from 2.43 to 2.64 Å, leading to a distorted octahedral BiO$_5$L coordination. Concerning strontium atoms, three different polyhedra are also observed. Two are characteristic of perovskite and rocksalt-type structures with 12 and 9 oxygens sur-
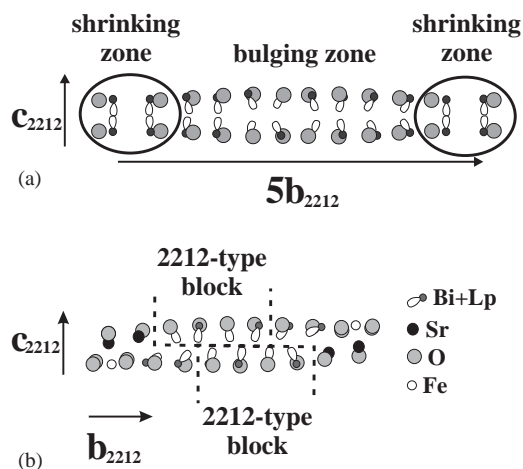
rounding strontium species respectively. Strontium atoms, namely Sr(11) in Table 3, exhibit a specific environment with 8 oxygens ranging from 2.67 to 3 Å. This unusual coordination is ascribed to the shearing zone in which these atoms sit. The partial strontium substitution by bismuth species detected during the refinements, in agreement with their location in the continuation of bismuth rows, could justify such a peculiar environment (Fig. 8).

These results show great similarities concerning the cation coordinations between the two members $m = 4, 5$ of the generic $[Bi_2Sr_3Fe_2O_9]_m[Bi_4Sr_6Fe_2O_{16}]$ collapsed family. Nevertheless, as emphasized in the previous single crystal study of the member $m = 4$ and in recent results obtained in the Bi–Sr–Fe–O system [1,4], cationic nonstoichiometries are observed from X-ray data refinements. Curiously in the case of the collapsed structures these disorders do not affect the framework of the shearing zone but only its cationic composition and/or
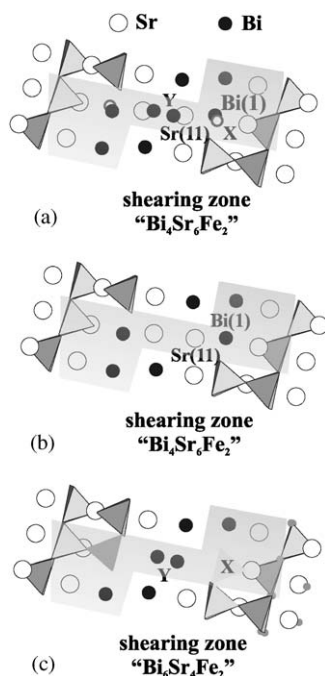
Fig. 9. Structural arrangement of $Bi_{14}Sr_{21}Fe_{12}O_{61}$ in the vicinity of the extra X and Y sites: (a) refined structure: both Bi(1), Sr(11), X and Y sites are represented. (b) the ideal structure: only the Bi(1) and Sr(11) sites are considered. (c) Only X and Y sites are considered.

the thickness of 2212-type slices. The single crystal refinement leads to an average model for the shearing zone (Fig. 9a). Two pairs of bismuth/strontium sites, Bi(1)/X and Y/Sr(11), with statistic occupancy were identified. Two hypothesis can be viewed to describe this disorder phenomenon. The first one considers the existence of local defects modifying only the structure of the shearing zone. In some parts of the crystal, X and Y sites could exist instead of Bi(1) and Sr(11). Two shearing zones drew in Fig. 9b and c are then expected in the compound. Note that, since the sum of the bismuth and strontium occupancies (Bi(1)+Y and X+Sr(11)) for the two atomic pairs is constant and equal to 1, the nonstoichiometry observed for the stair like compounds cannot be introduced with such model. The second hypothesis is based on the possible intergrowths between several m members of the $[Bi_2Sr_3Fe_2O_9]_m[Bi_4Sr_6Fe_2O_{15}]$ family within the crystal. In this interpretation, the structure of the shearing zone is fixed and corresponds to the model drawn in Fig. 9b while the thickness of the 2212 slices is variable inside the crystal. During an X-ray diffraction experiment the whole crystal is in the incident beam. So the refinement result corresponds to an average of all the different m values observed in the crystal and then lead to the existence of X and Y sites located in the continuation of the [SrO] and [BiO] segments respectively. To take into account such intergrowth phenomena, the chemical formula $x[Bi_2Sr_3Fe_2O_9]_{(m-1)}(1-x-y)[Bi_2Sr_3Fe_2O_9]_m$ $y[Bi_2Sr_3Fe_2O_9]_{(m+1)}[Bi_4Sr_6Fe_2O_{15}]$ should be used. Such

an analysis is consistent with the numerous intergrowth phenomena frequently observed from HREM images. Thus the behavior of these collapsed ferrites can be also compared to that the $m = 7$ collapsed 2212-cuprate $Bi_{16}Sr_{28}Cu_{17}O_{69+\delta}$, which deviates from the ideal formula $Bi_{18}Sr_{27}Cu_{16}O_{79}$, and exhibits numerous extended defects [15] representative of other m members. Consequently, the intergrowth approach allows us to explain the non stoichiometry frequently observed in such collapsed structures. Contrary to some strontium rich layered structures belonging to the Bi–Sr–Fe–O system, such as $Bi_{0.5}Sr_{2.5}FeO_5$ 1201-type [4] and $BiSr_3FeO_6$ 2201-type oxides [1], no cation Bi:Sr ordering mechanism was detected.

5. Conclusions

To summarize, cation deviations from ideal bismuth based modulated structures can be observed in the Bi–Sr–Fe–O system. They result into two structural mechanisms, either a Bi/Sr ordering or a periodic shearing. In the later case the undulated layers are always evidenced whereas in the ordered structures, in which the bismuth substitution are more significant, they have disappeared. So the collapsed structures could be viewed as alternate structural forms to the bismuth based nonmodulated ordered structures depending on the cation deviation with the parent modulated structure. Such a hypothesis needs some supplementary investigations like the synthesis of a nonmodulated ordered $(Bi, Sr)_2Sr_3Fe_2O_9$ 2212-type oxide and the control of oxygen stoichiometry during the thermal treatment.

In conclusion, a new member of the 2212-type stair like ferrites was isolated, showing the great ability of the Bi–Sr–Fe–O system to form such structures. In this respect iron can be compared to copper which also exhibit similar features. The detailed structure of the $m = 5$-member shows also its great complexity and also emphasizes the critical influence of the cationic composition upon the thickness of the 2212-slices. Finally, it highlights again the key role of the $6s^2$ electronic lone pair of bismuth in the generation of such frameworks.

References

[1] D. Pelloquin, M. Allix, C. Michel, M. Hervieu, B. Raveau, Phil. Mag. B 81 (11) (2001) 1669–1685.

[2] M. Hervieu, D. Pelloquin, C. Michel, M.T. Caldes, B. Raveau, J. Solid State Chem. 118 (1995) 227.

[3] V. Sedykh, I. Smirnova, B. Bagautdinov, K. Hagiya, M. Ohmasa, E. Suvorov, A. Dubovitskii, V. Shekhtman, Physica C 355 (2001) 87.

[4] M. Allix, D. Pelloquin, F. Studer, N. Nguyen, A. Wahl, A. Maignan, B. Raveau, J. Solid State Chem. 167 (2002) 48.

[5] M. Hervieu, C. Michel, N. Nguyen, R. Retoux, B. Raveau, Eur. J. Solid State Inorg. Chem. 25 (1988) 375.

[6] Y. Lepage, W.R. Mckinnon, J.M. Tarascon, P. Barboux, Phys. Rev. B 40 (1989) 6810.

[7] T. Fries, C. Steudtner, M. Schlichenmaier, S. Kemmler-Sack, T. Nissel, R.P. Huebener, J. Solid State Chem. 109 (1994) 88.

[8] O. Perez, H. Leligny, D. Grebille, P. Labbe, D. Groult, B. Raveau, J. Phys. Condens. Matter 7 (1995) 10003.

[9] V. Sedykh, F. Fujita, I. Smirnova, A. Dubovitskii, B. Narymbetov, V. Shekhtman, Jpn. J. Appl. Phys. 34 (1995) 4033.

[10] O. Perez, H. Leligny, D. Grebille, J.M. Greneche, P. Labbe, D. Groult, B. Raveau, Phys. Rev. B 55 (1997) 1236.

[11] D. Hechel, I. Felner, Physica B 262 (1999) 410.

[12] R. Retoux, C. Michel, M. Hervieu, N. Nguyen, B. Raveau, Solid State Commun. 69 (1989) 599.

[13] M. Hervieu, O. Perez, D. Groult, D. Grebille, H. Leligny, B. Raveau, J. Solid State Chem. 129 (1997) 214.

[14] O. Perez, H. Leligny, G. Baldinozzi, D. Grebille, M. Hervieu, P. Labbe, D. Groult, Phys. Rev. B 56 (1997) 5662.

[15] M. Hervieu, M.T. Caldes, C. Michel, D. Pelloquin, B. Raveau, J. Solid State Chem. 118 (1995) 357.

[16] J. Darriet, F. Weill, B. Darriet, X. Zhang, J. Etourneau, Solid State Commun. 86 (1993) 227.

[17] Y. Ikeda, H. Ito, S. Shimomura, Y. Oue, K. Inaba, Z. Hiroi, M. Takano, Physica C 159 (1989) 93.

[18] M. Hervieu, M.T. Caldes, S. Cabrera, C. Michel, D. Pelloquin, B. Raveau, J. Solid State Chem. 119 (1995) 169.

[19] J.M. Tarascon, W.R. Mc Kinnon, P. Barboux, D.M. Hwang, B.C. Babaly, L.H. Greene, G.H. Hull, Y. Lepage, N. Staffel, M. Giroud, Phys. Rev. B 38 (1988) 8885.

[20] R. Kilaas, Mac-Tempas software, distributed by N. Schryvers, EMAT Laboratory, University of Antwerp, Belgium, 1996.

[21] M. Burla, M. Camalli, B. Carrozzini, G.L. Cascarano, C. Giacovazzo, G. Polidori, R. Spagna, SIR2002, Institute of crystallography, Bari, Italia, 2002.

[22] V. Petricek, M. Dusek, Jana 2000, The crystallographic computing system, Institute of physics, Praha, Czech Republic, 2000.

[23] A. Duisenberg, L. Kroon-Batenburg, A. Shreurs, J. Appl. Crystal. 36 (2003) 220.